Volume 1 | Number 1 | Jan 2013 | Pages 1–100

Journal of
Materials Chemistry A

Materials for energy and sustainability
www.rsc.org/materialsA

Li⁺

ROYAL SOCIETY
OF CHEMISTRY

ROYAL SOCIETY
OF **CHEMISTRY**

www.rsc.org/materialsA

Journal of
Materials Chemisty A

COMMUNICATION

Thermoelectrics with Earth Abundant Elements: Low thermal conductivity and high thermopower in doped SnS

Qing Tan,[a] Li-Dong Zhao,[b] Jing-Feng Li,*,[a] Chao-Feng Wu,[a] Tian-Ran Wei,[a] Zhi-Bo Xing [a] and Mercouri G. Kanatzidis *,[b]

The thermoelectric properties of Ag-doped SnS samples synthesized by mechanical alloying and followed by spark plasma sintering were studied. We report that SnS possesses a high Seebeck coefficient of > +400 μV/K and Ag doping increases the carrier concentration by more than four orders of magnitude giving significantly improving electrical conductivity. The thermal conductivity falls below 0.5 W/mK at 873K and leads to a high *ZT* of 0.6. The data indicate that earth-abundant and environmentally-friendly SnS is a promising candidate for thermoelectric applications despite its relatively wide bandgap of 1.2 eV.

Thermoelectric effects enable direct conversion between thermal and electrical energy, which can be used for both power generation and refrigeration. The search for high-performance thermoelectrics with low cost and earth abundant elements is attracting significant attention because of energy efficiency, conservation and management concerns. The efficiency of thermoelectric devices is determined by the dimensionless figure of merit (ZT): $ZT = S^2\sigma T/\kappa$, where S is the Seebeck coefficient, σ is the electrical conductivity, T is the absolute temperature and κ is the thermal conductivity, respectively. Therefore, ideal thermoelectric materials require a perfect combination of a high power factor ($S^2\sigma$) and a low thermal conductivity (κ), which is the sum of the lattice conductivity component (κ_{lat}) and the electronic part (κ_{ele}).[1-3] Some compounds have been studied for several decades because of their high ZT values, such as PbTe-based and Bi_2Te_3-based materials.[4] Significant attention has focused on the earth-abundant, low-cost materials such as Cu_2S/Cu_2Se, BiCuSeO, $Ca_3Co_4O_9$, $Mg_2(Si,Sn)$, $Na_2Co_2O_4$ and $CuFeS_2$.[6-12]

Recently, the SnSe structure type was shown to have remarkably low thermal conductivity and high thermoelectric performance.[13] The same layered structure is adopted by the lighter analog, SnS, and this raises the question of studying its thermoelectric properties. Tin sulfide (SnS) is similar to the lead chalcogenides as both are in IV-VI groups, but its structure is different and its thermoelectric properties have not yet been systematically investigated.[14-17] However, SnS is an attractive compound, owing to its environmental compatibility, earth-abundant and low-cost. To date, SnS has been studied mainly for its optical properties including its photoconductivity and refractive index.[18-20] Parker and Singh calculated the band structure of SnS using the first-principles and deduced that SnS is an indirect semiconductor with a predicted high Seebeck coefficient, and a low thermal conductivity.[21] They suggested that p-type SnS is a potential thermoelectric material if it can be suitably doped, further motivating this work. The newly published calculation work by C. Bera *et. al* about SnS also supports the potentially good thermoelectric properties.[22]

To access the potential of SnS as a thermoelectric material, we synthesized this material using a mechanical alloying (MA) facile method and pressed MA-derived powders into pellets using spark plasma sintering (SPS).[23] Ag was selected as the p-type dopant. The synthetic details are given in the Supporting Information.

Figure 1(a) shows the crystal structure of SnS, which is orthorhombic with a *Pbmn* space group ($a = 4.33 \pm 0.02$ Å, $b = 11.19 \pm 0.05$ Å, and $c = 3.98 \pm 0.02$ Å).[21] SnS changes from the orthorhombic structure (α-phase) to a nearly tetragonal phase (β-phase) at 858 K with the first-order phase transition.[21, 24, 25] SnS
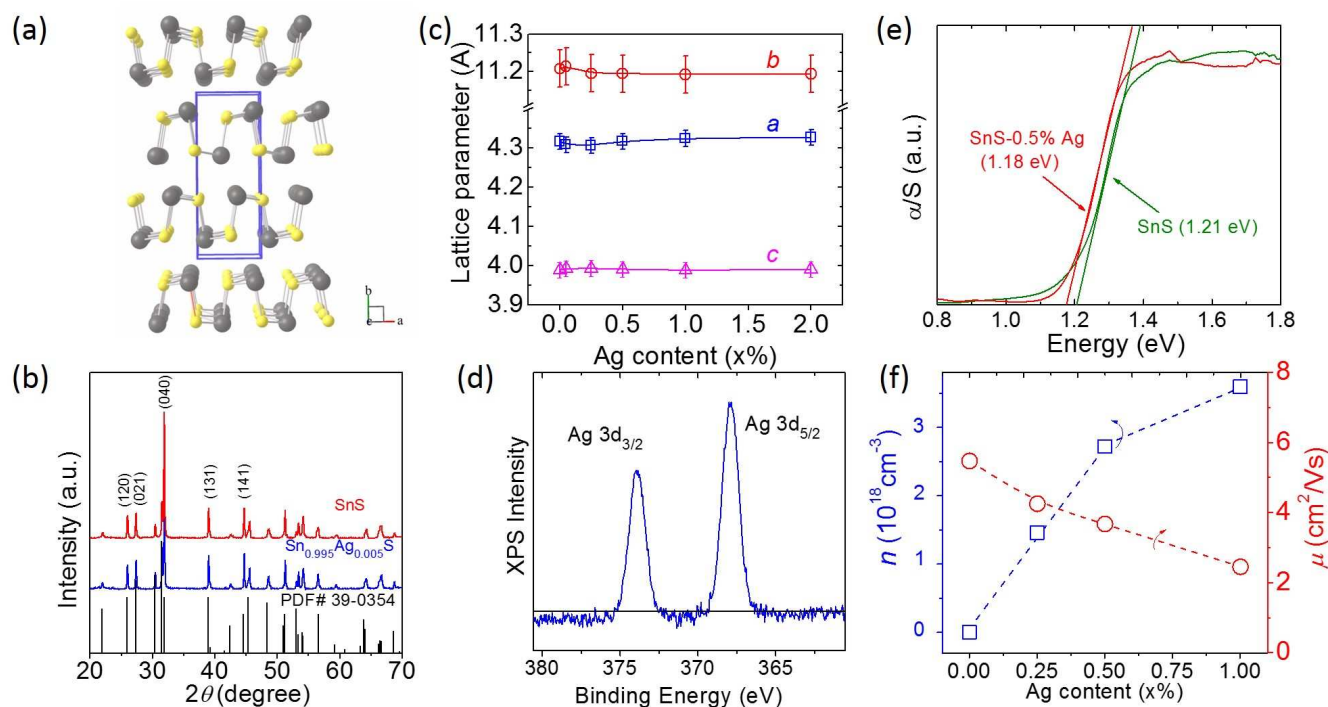
Figure 1. (a) The room temperature crystal structure of SnS, gray atoms represents Sn, yellow one is S, (b) X-ray diffraction patterns of SnS and SnS-0.5%Ag, (c) Ag content dependence of the lattice parameters, (d) X-ray photoelectron spectroscopy spectrum of the 3d orbitals for Ag element of the SnS-1%Ag, (e) optical absorption spectrum and energy bandgaps of SnS and SnS-0.5%Ag at room temperature, and (f) Ag content dependence of carrier concentration and mobility at room temperature.

has a distorted rock salt structure with a strongly layered character similar to SnSe.[13] The atoms in each layer are joined with the three nearest neighboring atoms by covalent bonds, forming accordion shaped corrugated slabs. The bonding forces between the layers are weak and mainly consist of long Sn - S interactions.

Figure 1(b) shows X-ray diffraction (XRD) patterns of the SnS and SnS-0.5%Ag samples and all major Bragg peaks can be indexed as SnS (PDF#39-0354), indicating that single-phase samples were successfully synthesized by MA and SPS. Figure 1(c) shows the lattice parameters as a function of the Ag content (x) for the SnS-x%Ag (x = 0, 0.05, 0.25, 0.5, 1 and 2), with rising Ag fractions the lattice parameter a and b remain unchanged, which is related to the similar radius of Ag^+ ions and Sn^{2+} ions (1.15 Å and 1.12 Å respectively). The presence of Ag was detected by X-ray photoelectron spectroscopy (XPS) and the binding energy of its 3d orbitals is shown in Figure 1(d). The measured binding energy of the Ag 3d orbitals is close to that in Ag_2S indicating the existence of Ag - S bond.[27, 28]

The optical absorption spectrum in Figure 1(e) shows that the bandgap of SnS is 1.21 eV, which shifts to a lower energy value (1.18 eV) when the Ag doping increases to 0.5%.[28-30] The Hall measurements show that the carriers in Ag doped SnS are holes and the carrier concentration (n) at 300 K increases rapidly from 1×10^{14} cm^{-3} for SnS to 1×10^{18} cm^{-3} for the sample with 1% Ag doping (The values of carrier concentration are displayed in Table 1). Correspondingly, the hole mobility shows a decreasing trend with rising Ag fractions, Figure 1(f). Collectively, XPS, energy bandgaps and charge transport measurements indicate that Ag^+ was successfully incorporated into the SnS lattice.

Consistent with the layered structure of SnS an obvious lamellar morphology was observed in field emission scanning electron microscopy (FESEM) images of its fractured surface (Figure 2(a)). The high magnification FESEM image shows that the thickness of each layer is only tens of nanometers, Figure 2(b). A series of zigzag-shaped stripes were also observed in the high resolution TEM (HRTEM) image in Figure 2(c) for the pristine SnS which correspond to the corrugated character of the SnS slab along the c-axis consistent with the crystal structure along the *c*-axis. The electron diffraction (ED) pattern in Figure 2(d) is also consistent with the XRD patterns and the orthorhombic structure of SnS.
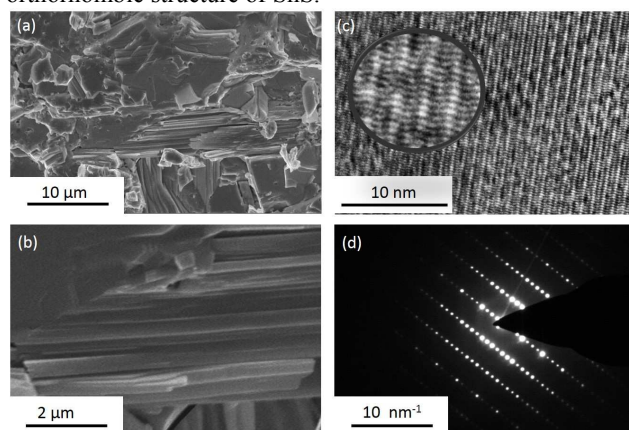
Figure 2. (a) FESEM image and (b) the lamellar grains of the fractured surface of SnS, (c) HRTEM image, inset shows the enlarged image and (d) electron diffraction pattern of SnS.

2 | J. Mater. Chem. A, 2014, **00**, 1-3

This journal is © The Royal Society of Chemistry 2014

The temperature dependence of the carrier concentration and mobility was investigated for both SnS and SnS-0.5%Ag samples, as shown in Figure 3(a). As stated above the carrier concentration of SnS was significantly enhanced by Ag doping. The following reaction is proposed for Ag doping:

$$Ag + S \xrightarrow{SnS} Ag_{Sn}^{'} + S_S^X + h^\bullet \qquad (1)$$
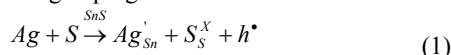
The increase of the electrical conductivity is attributed to holes $h^\bullet$, which were produced by reaction (1). In general, the carrier mobility decreases with an increasing carrier concentration since the Ag dopant scattered the holes. The carrier mobility values for the pristine SnS and SnS-0.5%Ag samples range from 7 - 12 $cm^2V^{-1}s^{-1}$. In both of the samples, the mobility increases with temperature up to 473 K, possibly due to activation barriers at the grain boundaries. At high temperatures, the hole mobility of SnS-0.5%Ag is generally limited by acoustic phonon scattering, for which the temperature dependence is given by the $\mu \propto T^r$ where r is 1.5 for nondegenerate semiconductors.[31] It should be noted that a carrier concentration upturn is observed at around 600 K. This increase in holes is also observed in p-type PbTe due to the contribution of the second valence band.[32] Similarly to PbTe, this apparent increase in the holes at high temperature in SnS could be the contribution of other valence bands which are lying close to the valence band maximum. Indeed, the present experimental results are consistent with the calculated band structure of SnS, in which the valence band maximum occurs along the $\Gamma-Z$ line and is composed of a relatively light-mass band, and one heavy-mass band sitting below the Fermi level.[22]

The electrical and thermal transport properties for pristine and Ag-doped SnS samples were measured over a wide temperature range from 300 to 923 K. As shown in Figure 3(b), the electrical conductivity for SnS-x%Ag (x = 0, 0.05, 0.25, 0.5, 1 and 2) increases with rising temperature, indicating a semiconducting transport behaviour. The electrical conductivityof SnS at 323 K is significantly increased by Ag

doping from 0.001 to ~3 S/cm, mainly due to the increased carrier concentration. SnS has a high Seebeck coefficient > +400 µV/K at room temperature, consistent with a p-type semiconductor, Figure 3(c). Even though Ag doping increased the electrical conductivity by four orders of magnitude the Seebeck coefficient maintains impressively high levels, Figure 3(c). To better understand the effect of Ag dopant on the valance band, the effective mass $m*$ was calculated using the following equations:[33]

$$S = \pm \frac{k_B}{e}\left[\frac{(s+5/2)F_{s+3/2}(\eta)}{(s+3/2)F_{s+1/2}(\eta)} - \eta\right]$$

$$= \frac{k_B}{e}\left[(s+\frac{5}{2}) + \ln\frac{2(2\pi m^* k_0 T)^{3/2}}{nh^3}\right] \qquad (2)$$

$$n = 4\pi(\frac{2m^* k_B T}{h^2})^{3/2}\frac{F_{1/2}(\eta)}{r_H} \qquad (3)$$

where s is the scatter factor, k_B is Boltzmann's constant, h is Planck's constant and e is electron charge. The calculated results are shown in Table 1, which displayed as the ratio of effective mass (m^*) to the electron mass (m_e). The $m*$ increased rapidly with increasing Ag content. The increasing $m*$ probably results from the heavy-mass band contribution due to deep-moving of Fermi level by Ag doping.

Table 1. The value of carrier concentration (n_H) and the ratio of effective mass (m^*) to the electron mass (m_e) for SnS-x%Ag samples at room temperature

Ag content (x)	0	0.05	0.25	0.5	1
$n_H(10^{18}cm^{-3})$	0.000137	0.00409	1.46	2.72	3.59
m^*/m_e	-	0.217	1.14	1.42	1.54
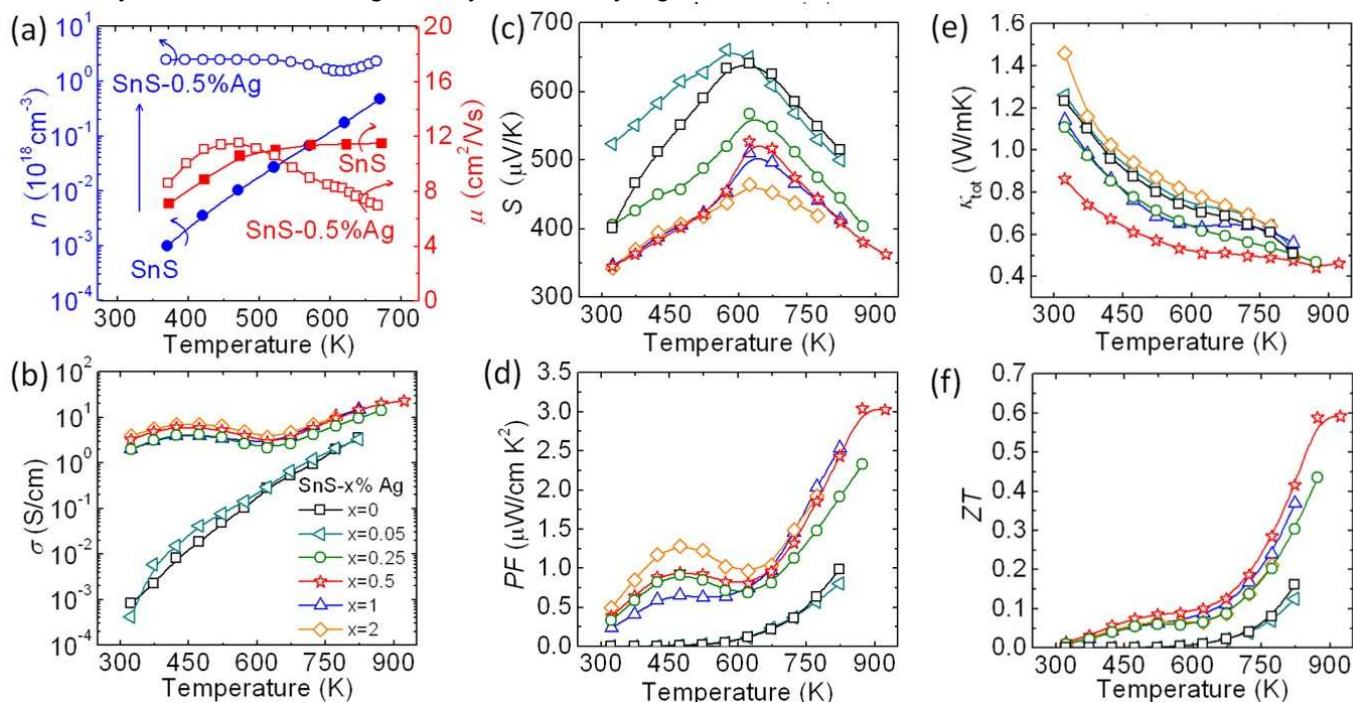
Figure 3. Temperature dependence of (a) carrier concentration and hole mobility, (b) electrical conductivity, (c) Seebeck coefficient, (d) power factor, (e) total thermal conductivity and (f) ZT of SnS-x%Ag (x=0, 0.05, 0.25, 0.5, 1 and 2) samples

The combined positive temperature−dependent electrical conductivity and Seebeck coefficient give high power factor ($S^2\sigma$) values at a high temperature, Figure 3(d); the highest power factor reaches ~3.0 $\mu Wcm^{-1}K^{-2}$ at 873K for the SnS-0.5%Ag sample.

Surprisingly, SnS has a very low thermal conductivity measured along the same direction as the electrical properties, which decreases from 1.25 W/mK at room temperature to 0.52 W/mK at 823K, as shown in Figure 3(e). The heat capacity, the thermal diffusivity, and samples density can be found in Figures S1 and Table S2. SnS shows the similar structure with that of SnSe, therefore, they may have a similar mechanism for their low thermal conductivity. The layered structure of SnSe features anomalously high Grüneisen parameters, which reflect the anharmonic and anisotropic bonding. The latter attributes are like also present in SnS. Point defects introduced in the structure by Ag doping contribute a further reduction in thermal conductivity. Indeed, the thermal conductivity was further reduced by Ag doping, and reaches as low as 0.40 W/mK at 873K for SnS-0.5%Ag sample. This is much lower than the ~1.20 W/mK of Na-doped PbS[34] and 2.0 W/mK of $Cu_4Mo_6S_8$.[35] A good experimental repeatability for these results was confirmed by the measurements in different places, Figure S2. It is interesting that the grain size growth is observed after Ag doping, but the reasons are not clear, see Figure S3. The effects on the 0.5% Ag sample may be complicated, such as bulk densities, microstructures, point defects and nano-precipitates. It is considered that two competitive reasons, Ag point scattering and grain size growth, make the thermal conductivity decrease until 0.5% Ag and then increase with future increasing Ag fractions up to 2% just happened at low temperature. The high temperature thermal conductivity varies little among different samples.

The very low thermal conductivity leads to a high *ZT,* Figure 3(f), the maximum *ZT* value for the SnS is ~ 0.16 at 873 K, and the SnS-0.5%Ag reaches *ZT* ~ 0.6 at 923 K. The present results indicate that Ag doping leads to an enhanced power factor and a lower thermal conductivity in SnS. The present *ZT* is impressive among *p*-type metal sulfides given the fact that SnS is a wide band gap compound. In fact, SnS exhibits the highest *ZT* value among *p*-type materials with bandgap above 1.0 eV.
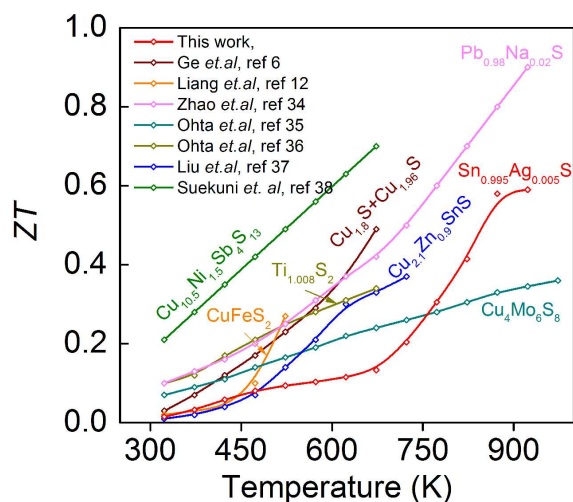
Figure 4. Temperature dependence of the *ZT* values of present SnS-0.5%Ag and other thermoelectric sulfides.

Conclusions

In summary, SnS is an interesting thermoelectric material because of its intrinsically low thermal conductivity and high Seebeck coefficient. The electrical conductivity of SnS can be significantly increased by Ag doping on Sn sites through increasing carrier concentration. The high performance realized in SnS system superior to the most of Pb-free sulfides, Figure 4. The *ZT* could be further enhanced by achieving higher carrier concentration through improved doping as well as through using approaches of microstructural optimization, nanostructuring control and compositional modification. The present results indicate that earth-abundant and environment-friendly SnS is a promising candidate for further thermoelectric investigations; both on its own merit and in connection with its better known congeners PbS and SnSe. The promising thermoelectric results reported here on SnS are not consist with the long held belief in the community that only narrow band gap semiconductors are worth investigating for low- and mid-temperature thermoelectric performance. In this regard the in-depth investigations on a much broader set of potential candidates should be widely concerned

Notes and references

aSchool of Materials Science and Engineering, State Key Laboratory of New Ceramics and Fine Processing, Tsinghua University, Beijing 100084, China

bDepartment of Chemistry, Northwestern University, Evanston, Illinois 60208, United States

Corresponding Authors:
jingfeng@mail.tsinghua.edu.cn;
m-kanatzidis@northwestern.edu
.

1   Bell, L. E. *Science* 2008, **321**, 1457.
2   Kanatzidis, M. G. *Chem. Mater*. 2010, **22**, 648.
3   Snyder, G. J.; Toberer, E. S. *Nature Mater*. 2008, **7**, 105.
4   Chen, G.; Dresselhaus, M. S.; Dresselhaus, G.; Fleurial, J. P.; Caillat, T. *Int. Mater. Rev*. 2003, **48**, 45.
5   Poudel, B.; Hao, Q.; Ma, Y.; Lan, Y.; Minnich, A.; Yu, B.; Yan, X.; Wang, D.; Muto, A.; Vashaee, D. *Science* 2008, **320**, 634.
6   Ge, Z. H.; Zhang, B. P.; Chen, Y.; Yu, Z. X.; Liu, Y.; Li, J. -F. *Chem. Commun*. 2011, **47**, 12697.
7   Liu, H.; Shi, X.; Xu, F.; Zhang, L.; Zhang, W.; Chen, L.; Li, Q.; Uher, C.; Day, T.; Snyder, G. J. *Nature. Mater*. 2012, **11**, 412.

8 (a) Liu, W.; Tang, X. F.; Sharp, J. *J. Phys. D: Appl. Phys* 2010, **43**, 085406.; (b) Liu, W.; Tan, X. J.; Yin, K.; Liu, H. J.; Tang, X. F.; Shi, J.; Zhang, Q. J.; Uher, C. *Phys. Rev. Lett.* 2012, **108**, 166601.

9 Nong, N. V.; Pryds, N.; Linderoth, S.; Ohtaki, M. *Adv. Mater.* 2011, **23**, 2484.

10 Heinrich, C. P.; Day, T. W.; Zeier, W. G.; Snyder, G. J.; Tremel, W. *J. Am. Chem. Soc.* 2014, **136**, 442.

11 Zhao, L. D. ; Berardan, D. ; Pei, Y. L. ; Byl, C. ; Pinsard-Gaudart, L. ; Dragoe, N. *Appl. Phys. Lett.* 2010 **97**, 092118

12 Liang, D.; Ma, R.; Jiao, S.; Pang, G.; Feng, S. *Nanoscale* 2012, **4**, 6265.

13 Zhao, L. D.; Lo, S. H.; Zhang, Y. S.; Sun, H.; Tan, G. J.; Uher, C.; Wolverton, C.; Dravid, V. P.; Kanatzidis, M. G. *Nature* 2014, **508**, 373.

14 Nassary, M. M. *J. Alloys Compd.* 2005, **398**, 21.

15 Patel, T. H.; Vaidya, R.; Patel. S. G. *High Pressure Res.* 2003, **23**, 417.

16 Nariya, B. B.; Dasadia, A. K.; Bhayani, M. K.; Patel, A. J.; Jani, A. R. *Chalcogenide. Lett.* 2009, **6**, 549.

17 Jayasree, Y.; Chalapathi, U.; Bhaskar, P. U.; Raja, V. S. *Appl. Surf. Sci.* 2012, **258**, 2732

18 Gao, C.; Shen, H. -L.; Sun. L. *Appl. Surf. Sci.* 2011, **257**, 6750.

19 Sohila, S.; Rajalakshmi, M.; Muthamizhchelvan, C.; Kalavathi, S.; Ghosh, C.; Divakar, R.; Venkiteswaran, C. N.; N Muralidharan, . G.; Arora, A. K.; Mohandas, E. *Mater. Lett.* 2011, **65**, 1148.

20 Shaposhnikov, V. L.; Krivosheeva, A. V.; Borisenko. V. E.; Lazzari, J. -L. *Science Jet* 2012, **1**, 15.

21 Parker, D.; Singh, D. J. *J. Appl. Phys.* 2010, **108**, 083712.

22 Bera, C. ; Jacob, S.; Opahle, I. ; Gunda, N. S. H. ; Chmielowski, R. ; Dennlerb, G. ; Madsen, J. K. H. *Phys. Chem. Chem. Phys.*, 2014, DOI: 10.1039/C4CP02871F.

23 Tan, Q. ; Li, J. –F. *J. Electron. Mater.* 2014, **43**, 2435

24 Chattopadhyay, T.; Werner, A.; von Schnering, H. G.; Pannetier, J. *Rev. Phys. Appl.* 1984, **19**, 807

25 Chattopadhyay, T.; Pannetier, J.; Von Schnering, H. G. *J. Phys. Chem. Solids* 1986, **47**, 879

26 Romand, R.; Roubin, M.; Deloume, J. P. *J. Electron Spectrosc. Relat. Phenom.* 1978, **13**, 229

27 Naumkin, A. V.; Kraut-Vass, A.; Gaarenstroom, S. W.; Powell, C. J.; NIST X-ray Photoelectron Spectroscopy Database, http://srdata.nist.gov/xps/selEnergyType.aspx, 2012**.**

28 Madelung, O.; Rössler, U.; Schulz, M. *Landolt-Börnstein-Group III Condensed Matter*; Springer: Verlag, 1983.

29 Vogel, R.; Hoyer, P.; Weller. H. *J. Phys. Chem.* 1994**, 98,** 3183

30 von der Oster, M. *Landolt-Bornstein* 1982, **172**, 156.

31 Zevalkink, A.; Toberer, E. S.; Zeier, W. G.; Flage-Larsen, E.; Snyder, G. J. *Energy Environ. Sci.* 2011, **4**, 510.

32 Pei, Y.; Shi, X.; LaLonde, A.; Wang, H.; Chen, L.; Snyder, G. J. *Nature* 2011, **473**, 66.

33 Rowe, D. W. *Materials, Preparation, and Characterizition in Thermoelectrics*, CRC Press, New York, 2012

34 Zhao, L. D.; He, J. Q.; Hao, S. Q.; Wu, C.-I.; Hogan, T. P.; Wolverton, C.; Dravid, V. P.; Kanatzidis, M. G. *J. Am. Chem. Soc*. 2012, **134**, 16327.

35 Ohta, M.; Yamamoto, A.; Obara, H. *J. Electron. Mater.* 2010, **39**, 2117.

36 Ohta, M.; Satoh, S.; Kuzuya, T.; Hirai, S.; Kunii, M.; Yamamoto, A. *Acta Mater.* 2012, **60**, 7232.

37 Liu, M.; Huang, F.; Chen, L. D.; Chen. I. *Appl. Phys. Lett.* 2009, **94**, 202103.

38 Suekuni, K. ; Tsuruta, K. ; Kunii, M. ; Nishiate, H. ; Nishibori, E. ; Maki, S. ; Ohta, M. ; Yamamoto, A. ; Koyano, M. *J. Appl. Phys.* 2013, **113**, 043712.

This journal is © The Royal Society of Chemistry 2014

J. Mater. Chem.A, 2014, **00**, 1-3 | **5**

Title "Thermoelectrics with Earth Abundant Elements: Low thermal conductivity and high thermopower in doped SnS"

The table of contents entry
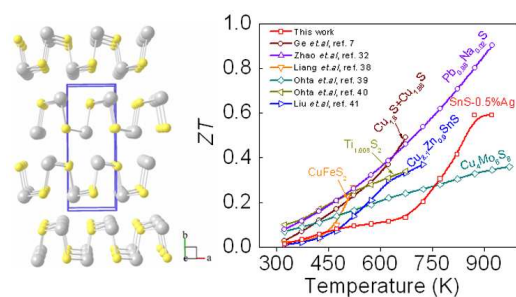
We present that earth-abundant and environmentally-friendly SnS is a promising candidate for thermoelectric applications for its high *ZT* of 0.6 despite its relatively wide band gap of 1.2 eV. Ag doping significantly improved electrical conductivity but maintained the Seebeck coefficient above 400 µV/K and the thermal conductivity below 0.45 W/mK at 873K.